Spatiotemporal spin dynamics of two-dimensional electron gas with ballistic motion in persistent spin helix state

Jun Ishihara ◉,[1,][*] Takuya Suzuki,[1] Go Kitazawa,[1] Takachika Mori,[1] Yuzo Ohno,[2] and Kensuke Miyajima ◉[1]

[1]*Department of Applied Physics, Tokyo University of Science, Tokyo 125-8585, Japan*
[2]*Graduate School of Pure and Applied Sciences, University of Tsukuba, Tsukuba 305-8573, Japan*

The spatiotemporal spin dynamics of two-dimensional electron spins with ballistic motion in a GaAs quantum well is investigated using time- and spatially resolved magneto-optical Kerr rotation measurements. The ballistic movement of photoexcited spins, which maintains the width of the excitation spot size, results in a wave-packet-like motion of the spin distribution. The time evolution of the spin distribution measured at different excitation intensities reveals that the spin diffusion slows down and the wave-packet-like motion disappears at higher photoexcited spin densities, at which the spin distribution converges to the helical spin mode observed in the diffusive regime. The variation in the spatiotemporal spin distribution can be controlled by spin diffusion, while the spin precession length is determined by the strength of the spin-orbit interaction.

I. INTRODUCTION

The persistent spin helix (PSH) state, in which the spatial spin rotation is robust against all spin-independent scattering [1,2], has attracted much attention owing to its long lifetime and controllable spin state. The PSH state with a helical spin texture in a (001)-grown quantum well (QW) with zinc-blende structure occurs [3] when the Rashba [4] and Dresselhaus [5] spin-orbit (SO) interactions are balanced. D'yakonov-Perel' (DP) spin relaxation [6], which is the main mechanism for spin dephasing, is completely suppressed in the PSH field, which has an exact SU(2) symmetry. The long-lived spin texture in the PSH opens an avenue for functional spin-related devices. The direct observation of a helical spin texture [3], fine-tuning of the PSH by out of plane gate voltages [7,8], long-distance transport of the PSH by drift currents [9], and long-lived ensemble-averaged spin state [10–13] have been demonstrated experimentally in the PSH state. Its dynamics has also been investigated under diffusive [3,8,14–17] and drift transport [18–21] using time- and spatially resolved optical spin measurements. In addition, it has been theoretically shown that the PSH lifetime can be extended by choosing a proper crystal orientation of the QW plane that is more robust than the PSH in the (001) plane [22–24]. Because the spatial spin state depends only on the displacement in the PSH state, almost all the optical experiments have been performed under diffusive electron motion.

In comparison, because coherent spin precession is observed in the time domain under ballistic electron motion [25–28], the temporal spin information from coherent precession is also useful for revealing fast spin flipping and the rapid formation of a helical spin texture. The conversion of spatial spin precession information into coherent spin precession information in the time domain in the ballistic regime allows the SO effective magnetic fields to be characterized without the need for high spatial resolutions. In a previous study, we reported the time evolution of ensemble-averaged spins with ballistic electron motion using the time-resolved Kerr rotation method with a large spot size and estimated the SO coefficients by analyzing the precession frequency in the PSH regime [28]. Although this method allows us to obtain the strength of the SO effective magnetic fields in all directions through the observation of coherent oscillations in the ballistic regime, the spin-diffusion information is lost. In this study, we investigate the spatiotemporal evolution of high-mobility two-dimensional electron spins with ballistic motion using the time- and spatially resolved Kerr rotation (KR) technique to clarify the fast propagation of spins in the PSH regime. The time evolution of the spin distribution shows a wave-packet-like motion with a different spin precession from the reported time evolution of the spin distribution in the diffusive regime. From the temporal changes in the spin distribution and spin precession frequency, the spin-diffusion velocity and strength of the SO effective magnetic field are estimated simultaneously. In addition, we observe the variation in the time evolution of the spin distribution in the transition from ballistic to diffusive electron motion. The experimental results are reproduced in a spin-diffusion coefficient-dependent spin dynamics calculation using the Monte Carlo method.

II. EXPERIMENTAL METHODS

A single-sided modulation-doped 20 nm GaAs/AlGaAs QW was grown on a semi-insulating (001) GaAs substrate using molecular beam epitaxy. A 20 nm thick highly Si-doped AlGaAs layer was used with a 35 nm thick undoped AlGaAs spacer layer on top of the QW to generate a
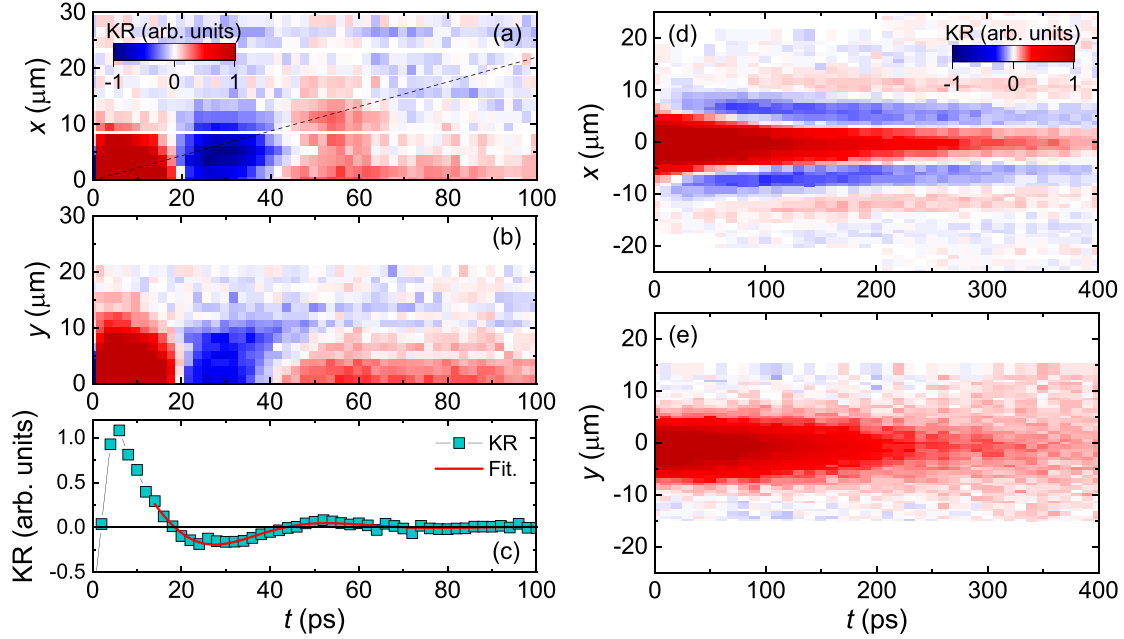
---

[*]j.ishihara@rs.tus.ac.jp

FIG. 1. Time evolution of the spin distribution. KR maps corresponding to (a) $S_z(x, 0, t)$ and (b) $S_z(0, y, t)$ under experimental conditions for ballistic electron motion. The dashed line represents $x = v_s t$. (c) Time-resolved KR on the $x = v_s t$ line in (a). The solid line is a fitting curve. (d) $S_z(x, 0, t)$ and (e) $S_z(0, y, t)$ for diffusive electron motion.

high-mobility two-dimensional electron gas (2DEG). The 2DEG density n, electron mobility μ, and electron diffusive coefficient D_e determined using Hall and conductivity measurements at 5 K after light irradiation were 4.1×10^{15} m^{-2}, 130 m^{2}V^{-1}s^{-1}, and 1.92 m^2/s, respectively. The mean free path was estimated to be 13.7 μm. The asymmetric profile of the QW in this quantum structure induced a large Rashba SO interaction, resulting in SO fields that were close to the PSH. The time evolution of the spin distribution was measured using a time- and spatially resolved magneto-optical KR technique. A pulse train generated by a mode-locked Ti:sapphire laser with a repetition rate of 82 MHz and pulse duration of approximately 1.5 ps was split into the pump and probe beams. The helicity of the circularly polarized pump beam was modulated at $f = 50.147$ kHz using a photoelastic modulator. The linearly polarized probe beam was modulated using an acousto-optical modulator at $f_a = 51$ kHz. The pump and probe beams were focused on the sample surface using an aspheric lens with 26 mm focal length. The relative delay time t and relative position (x//[1$\bar{1}$0] and y//[110]) between the pump and probe beams were automatically controlled using a mechanical delay line and a scanning mirror, respectively. The e^{-2} spot sizes of the pump and probe beams were 7.1 and 12.6 μm, respectively. Polarized electron spins along the growth direction were optically excited by the circularly polarized pump beam, which had a Gaussian distribution. The ensemble-averaged out of plane spin component $S_z(x, y, t)$ within the Gaussian spot of the probe beam was detected as a KR signal using a balanced photoreceiver and a lock-in amplifier tuned at $f_a - f$. Optical measurements were performed at 7 K using a cryostat with an optical access. The carrier density in the QW n_{PLE} determined by the Stokes shift between the photoluminescence and photoluminescence excitation spectra was 3.5×10^{15} m^{-2}.

III. RESULTS AND DISCUSSION

Figures 1(a) and 1(b) show the time evolution of the KR distribution along the x and y directions corresponding to $S_z(x, 0, t)$ and $S_z(0, y, t)$, respectively, at the pump intensity of 7 μW. As the time increases, the spin distribution moves along the x direction with the same spin distribution width it has at the time of excitation and undergoes precession by the large SO effective magnetic field. This wave-packet-like electron spin motion, which undergoes a different spatiotemporal evolution from that in the diffusive regime shown in Figs. 1(d) and 1(e) (the experimental conditions for the diffusive regime are described in the Supplemental Material [29]) indicates that the spins move at a constant velocity without scattering. In contrast to the spin precession observed in the x direction, the spins moving along the y direction maintain their spin state after flipping once, as shown in Fig. 1(b). The observed anisotropic time evolution of the spin distribution is caused by the coexistence of the Rashba and Dresselhaus SO effective magnetic fields. The precession angular frequency due to the effective magnetic field depends on the wave vector and is given by

$$\Omega(\theta) = \frac{2k_{\text{F}}}{\hbar} \sqrt{\alpha^2 + \tilde{\beta}^2} \sqrt{1 - \sin 2\varphi \cos 2\theta}. \tag{1}$$

Here, $\hbar$ is the reduced Planck constant; $k_{\text{F}} = \sqrt{2\pi n_{\text{PLE}}}$ the Fermi wave number; α the Rashba coefficient; and $\tilde{\beta} = \beta_1 - \beta_3$, where β_1 and β_3 are the linear and cubic Dresselhaus coefficients, respectively. θ is the angle between the wave vector and the [1$\bar{1}$0] crystal axis and $\varphi = \arctan(\alpha/\tilde{\beta})$. The third angular harmonics of the SO fields are ignored. In the sample structure used in this experiment, band bending occurs at the top side of the QW. The combination of the Rashba ($\alpha < 0$) and Dresselhaus ($\tilde{\beta} > 0$) SO effective

magnetic fields therefore act on electron spins moving along the x direction ($//[1\bar{1}0]$), whereas the two SO effective magnetic fields cancel out for spins moving along the y direction ($//[110]$). For the latter spins, the reduction of the SO effective magnetic field to almost zero results in the absence of spin precession even after 20 ps. The spin-diffusion velocity is extracted as $v_s = 0.22 \pm 0.02\,\mu m/ps$ by following the center of the moving spin packet. The Fermi velocity of $v_F = 0.26\,\mu m/ps$ estimated from $\hbar\sqrt{2\pi n_{\text{PLE}}}/m$ using the measured carrier density is close to v_s. Therefore, we find that the photoexcited electron spins move almost without scattering with the constant velocity of v_s in the radial direction. The difference between the obtained v_s and v_F might be caused by the enhancement of electron-electron scattering by photoexcited electrons [28]. Figure 1(c) shows the time evolution of the spins at $x = v_s t$ in Fig. 1(a). By fitting $S_z(x = v_s t, y = 0, t) = A\exp(-t/\tau_s)\cos\Omega t$ to the experimental results, the precession angular frequency is obtained as $\Omega = 0.124\,rad/ps$. Using the obtained v_s and Ω, we estimate the spin precession length to be $\lambda_{SO} = 2\pi v_s/\Omega = 11.15\,\mu m$ and the SO parameter to be $-\alpha + \tilde{\beta} = \pi\hbar^2/m\lambda_{SO} = 3.2\,meV\,\text{Å}$, which is a reasonable value for GaAs/AlGaAs asymmetric QW compared with previous reports [3,8,19]. To validate the values obtained in this experiment, we directly observe the helical spin mode in the diffusive regime using high-resolution measurements. The spin precession length directly estimated from the residual helical spin mode is $11.2\,\mu m$ (see Fig. S1 in the Supplemental Material [29]), which is consistent with the value obtained in this experiment. This indicates that the present measurement simultaneously provides not only the spin-diffusion velocity but also the spin precession length due to the SO field.

As shown in Fig. 1(a), the spins at $(x, y) = (0, 0)$ exhibit rotation with time despite the outward diffusion of the photoexcited electron spins at the spatial origin. This signal is induced by the inflow of spins excited with a Gaussian distribution into the probe position, which depends on the sigma widths of the convolution between the pump and probe beam Gaussian distributions σ_{eff}. Figure 2(a) shows the time evolution of spins measured under the two different σ_{eff} conditions of 18 and 3.6 μm. At $\sigma_{\text{eff}} = 18\,\mu m$, spin precession is clearly observed. However, the spin precession disappears rapidly at $\sigma_{\text{eff}} = 3.6\,\mu m$, which corresponds to the data for $S_z(0, 0, t)$ extracted from Fig. 1(a). The spin signal probed at distance r from the pump position and the delay time $t = r/v_F$ in the ballistic regime is given by [30]

$$s_z(x, y, t) = s_{z0}\cos[\Omega(\theta)t]\frac{1}{r}\delta(r - v_F t), \quad (2)$$

where s_{z0} is the initial amplitude of the spin z component and $r = \sqrt{x^2 + y^2}$, $\theta = \arctan(y/x)$. The probed spin component s_z of the spin distribution in the experiment includes contributions from the initial spin probability density, which depends on the position. For photoexcitation with a Gaussian distribution, the probed spin signal due to the spin excited at position (X, Y) is

$$s_z(x, y, t) = s_{z0}\exp\left(-\frac{R^2}{2\sigma_{\text{eff}}^2}\right)\cos[\Omega(\theta')t]\frac{1}{r'}\delta(r' - v_F t). \quad (3)$$
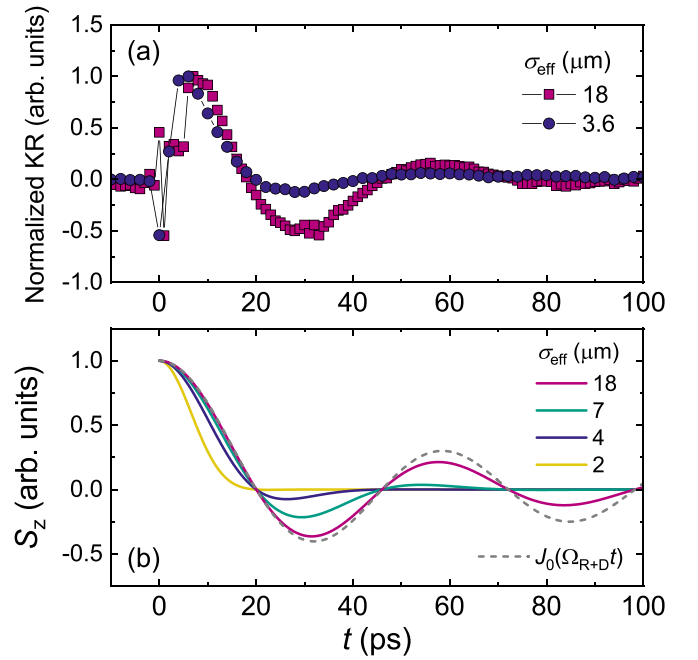

FIG. 2. (a) Time-resolved KR signal measured under different convoluted sigma widths σ_{eff}. The data for $\sigma_{\text{eff}} = 18\,\mu m$ are from Ref. [28]. (b) $S_z(t)$ calculated at various σ_{eff} using Eq. (4). The dashed line denotes $J_0(\Omega_{R+D}t)$.

Here, $R^2 = X^2 + Y^2$, $r' = \sqrt{(x-X)^2 + (y-Y)^2}$, and $\theta' = \arctan(Y-y/X-x)$. For the PSH state ($\tilde{\beta} = -\alpha$), the magnitude of the precession frequency is $\Omega(\theta') = \Omega_{R+D}\cos\theta'$, where $\Omega_{R+D} = 2k_F(-\alpha + \tilde{\beta})/\hbar$. Consequently, the observed time evolution of spins at the spatial origin $(0, 0)$ obtained as the summation of contributions from $R = r' = v_F t$ is given by

$$S_z(t) = S_{z0}\exp\left(-\frac{v_F^2 t^2}{2\sigma_{\text{eff}}^2}\right)J_0(\Omega_{R+D}t), \quad (4)$$

where J_0 is the zero-order Bessel function of the first type. Figure 2(b) shows the calculated $S_z(t)$ for different values of σ_{eff}. The calculations reproduce the experimentally observed disappearance of the spin precession at small spot sizes. This indicates that the observed one-dimensional spin distribution includes not only the electron spins moving along the observation axis but also those moving perpendicular to the observation axis. As a result, spin rotation due to the inflow of spins is also observed around the spatial origin in the spin distribution in the y direction [Fig. 1(b)], while no spin rotation is observed under diffusive electron motion [Fig. 1(d)]. This effect due to the inflow of spins becomes weaker as the probe position becomes farther from the pump position; this is because the direction of electron motion arriving at the probe position becomes parallel to the observation axis in the ballistic regime. In the diffusive regime, a similar effect of electron motion that is perpendicular to the observation axis on the spin dynamics has been reported as a modulation of the spin precession frequency under an external magnetic field [31].

To investigate the spin dynamics in the transition region from ballistic motion to diffusive motion, we measure the time evolution of the spin distribution by increasing the pump intensity. The high-density excitation of electrons and the
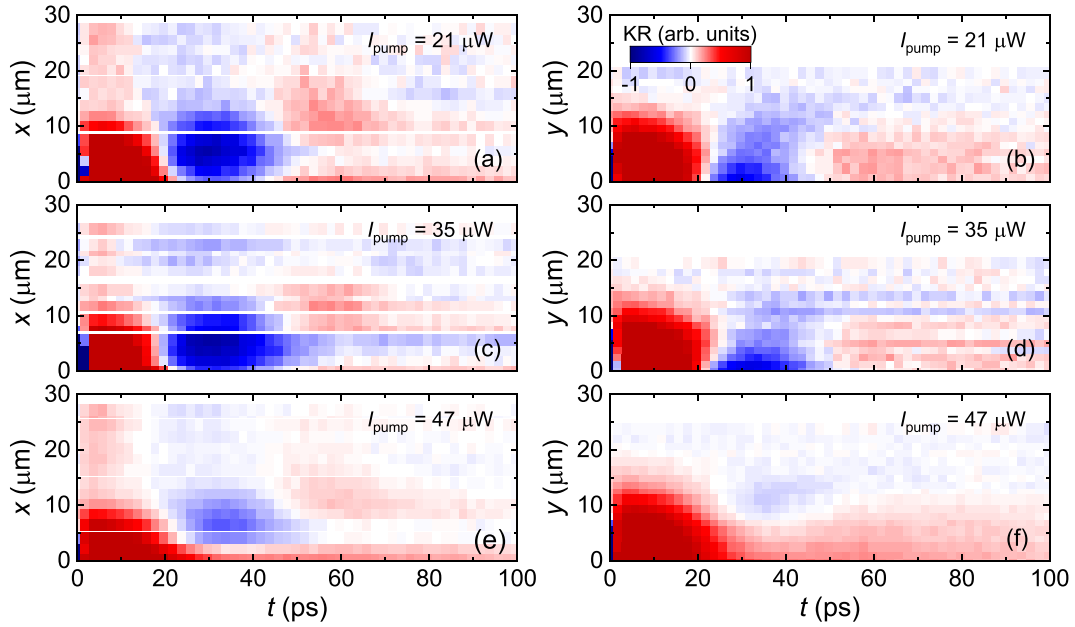
FIG. 3. Excitation intensity I_{pump} dependence of time evolution of spin distribution. (a) $S_z(x, 0, t)$ and (b) $S_z(0, y, t)$ at $I_{\text{pump}} = 21\,\mu\text{W}$, which is three times larger than in the experiment shown in Figs. 1(a) and 1(b). (c), (d) are measured at $I_{\text{pump}} = 35\,\mu\text{W}$. (e), (f) are measured at $I_{\text{pump}} = 47\,\mu\text{W}$.

detuning excitation energy from the resonant excitation enhance electron-electron scattering [28,32]. Figure 3 shows the time evolution of the spin distributions under different excitation intensities. The time evolution of the spin distribution is observed to depend on the excitation intensity. Increasing the excitation intensity increases the photoexcited carrier density, reduces the spin-diffusion velocity, and eliminates the wave-packet-like spatial spin motion. At higher spin densities, the spin distribution along the x direction tails off with time and converges to the helical spin mode observed in the diffusive regime shown in Fig. 1(d). In contrast, the spin flip of electrons moving along the y direction and spin precession at the spatial origin almost disappear. These results suggest that the high-density photoexcited electrons enhance the scattering rate of spins and result in a transition to diffusive electron motion, which is consistent with a previous report [28]. Another effect of increasing excitation density on the spin distribution is the modulation of SO interactions due to optical doping [17]. However, in the present study, the modulation of SO interaction is negligible because the excitation density is several orders of magnitude smaller than that in Ref. [17]. The absence of SO modulation due to optical doping is also supported by the fact that the spin precession length obtained from the results shown in Figs. 1(a) and 1(c) is consistent with that obtained from the helical spin mode in the case of a higher excitation density (Fig. S1(b) in the Supplemental Material [29]). To confirm whether this temporal variation of the spin distribution is mainly due to the decrease in the spin-diffusion coefficient, we calculate the spatiotemporal evolution of spins in the presence of SO interactions using a Monte Carlo simulation. In the simulation, the time evolution of the spin $\mathbf{S}(t)$ is given by $d\mathbf{S}(t)/dt = \mathbf{\Omega} \times \mathbf{S}$. Scattering occurs with an average scattering time of τ, and the direction of electron motion changes randomly due to the

scattering. The electron spins are initially polarized along the z direction with a Gaussian distribution and the value of $\langle S_z \rangle$ is calculated using a Gaussian probability density function with the width of the probe beam in correspondence to the optical excitation in the experiment. The SO parameters of $\alpha = -1.76\,\text{meV}\,\text{Å}$ and $\tilde{\beta} = -\gamma\langle k_z^2 \rangle + \gamma k_F^2/4 = 1.44\,\text{meV}\,\text{Å}$ used in the calculation are determined from the experimental value of $-\alpha + \tilde{\beta} = 3.2\,\text{meV}\,\text{Å}$, and the calculated value of $\langle k_z^2 \rangle = 1.86 \times 10^{16}\,\text{m}^{-2}$ and the reported bulk Dresselhaus coefficient of $\gamma = -11\,\text{eV}\,\text{Å}^3$ [33] are used. The spin dynamics are calculated for various values of the scattering time $\tau = 2D_s/v_F^2$, where D_s is the spin-diffusion coefficient. Figure 4 shows the time evolution of the calculated spin distributions $S_z(x, 0, t)$ and $S_z(0, y, t)$ at different D_s. The simulation results for the excitation dependence of the spin-diffusion coefficient reproduce the experimental results [Figs. 1(a), 1(b), and 3(a)–3(f)]. In the calculation results for the $D_s = D_e$ condition, the spins move with the wave-packet-like motion observed in the experiment, as shown in Figs. 4(a) and 4(b). In addition, the spin flip for electrons moving along the y direction and the spin rotation at the spatial origin are also reproduced. As D_s decreases [Figs. 4(c)–4(f)], the wave-packet-like electron motion, spin flip in the y direction, and spin rotation at the spatial origin disappear, which is in qualitative agreement with the experimental results for higher excitation densities. These results show that the spatiotemporal variation of the spin distribution is determined by the spin scattering rate and can be controlled by the excitation intensity.

IV. CONCLUSIONS

In conclusion, we directly observe the time evolution of the spin distribution under ballistic electron motion in a
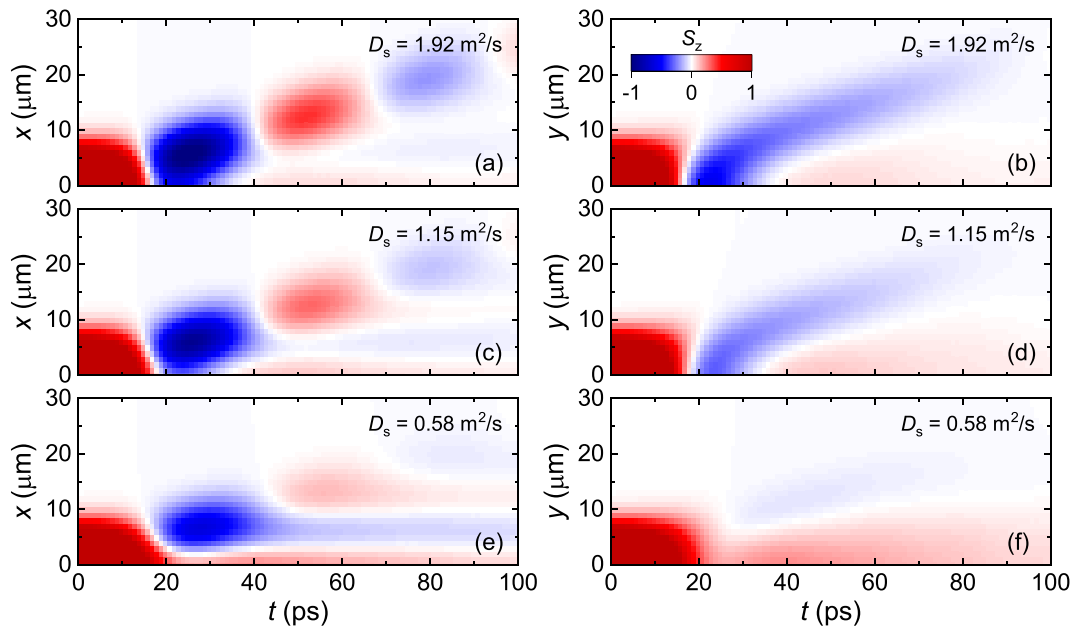
FIG. 4. Simulation of $S_z(x, 0, t)$ and $S_z(0, y, t)$ under various D_s values. (a), (b) correspond to the condition of $D_s = D_e = 1.92 \, \text{m}^2/\text{s}$, (c), (d) $D_s = 1.15 \, \text{m}^2/\text{s}$, and (e), (f) $D_s = 0.58 \, \text{m}^2/\text{s}$.

high-mobility 2DEG. The photoexcited electron spins spread with the background 2DEG diffusion velocity. The time evolution of the spin distribution shows that the wave-packet-like motion under the ballistic regime is quite different from that in the diffusive regime. From the wave-packet-like motion and precession of the spin distribution, we can extract not only the strength of the SO parameter but also the spin-diffusion velocity simultaneously. As the electron spin motion scattering rate increases with increasing spin excitation intensity, spin diffusion slows down and the wave-packet-like motion disappears, causing significant changes in the spatiotemporal spin distribution. These results will be helpful for further

understanding the fast propagation of spins under the ballistic and diffusive regimes, as well as for the utilization of the spatiotemporal information in the PSH state in semiconductor quantum structures.

ACKNOWLEDGMENTS

[1] J. Schliemann and D. Loss, Phys. Rev. B **68**, 165311 (2003).

[2] B. A. Bernevig, J. Orenstein, and S. C. Zhang, Phys. Rev. Lett. **97**, 236601 (2006).

[3] M. P. Walser, C. Reichl, W. Wegscheider, and G. Salis, Nat. Phys. **8**, 757 (2012).

[4] E. I. Rashba, Sov. Phys. Solid State **2**, 1109 (1960).

[5] G. Dresselhaus, Phys. Rev. **100**, 580 (1955).

[6] M. I. D'yakonov and V. I. Perel', Sov. Phys. JETP **33**, 1053 (1971).

[7] M. Kohda, V. Lechner, Y. Kunihashi, T. Dollinger, P. Olbrich, C. Schönhuber, I. Caspers, V. V. Bel'kov, L. E. Golub, D. Weiss, K. Richter, J. Nitta, and S. D. Ganichev, Phys. Rev. B **86**, 081306(R) (2012).

[8] J. Ishihara, Y. Ohno, and H. Ohno, Appl. Phys. Express **7**, 013001 (2014).

[9] Y. Kunihashi, H. Sanada, H. Gotoh, K. Onomitsu, M. Kohda, J. Nitta, and T. Sogawa, Nat. Commun. **7**, 10722 (2016).

[10] J. D. Koralek, C. P. Weber, J. Orenstein, B. A. Bernevig, S. C. Zhang, S. Mack, and D. D. Awschalom, Nature (London) **458**, 610 (2009).

[11] S. Z. Denega, T. Last, J. Liu, A. Slachter, P. J. Rizo, P. H. M. van Loosdrecht, B. J. van Wees, D. Reuter, A. D. Wieck, and C. H. van der Wal, Phys. Rev. B **81**, 153302 (2010).

[12] J. Ishihara, M. Ono, Y. Ohno, and H. Ohno, Appl. Phys. Lett. **102**, 212402 (2013).

[13] F. G. G. Hernandez, G. J. Ferreira, M. Luengo-Kovac, V. Sih, N. M. Kawahala, G. M. Gusev, and A. K. Bakarov, Phys. Rev. B **102**, 125305 (2020).

[14] G. Salis, M. P. Walser, P. Altmann, C. Reichl, and W. Wegscheider, Phys. Rev. B **89**, 045304 (2014).

[15] J. Ishihara, Y. Ohno, and H. Ohno, Jpn. J. Appl. Phys. **53**, 04EM04 (2014).

[16] P. Altmann, M. P. Walser, C. Reichl, W. Wegscheider, and G. Salis, Phys. Rev. B **90**, 201306(R) (2014).

[17] F. Passmann, S. Anghel, T. Tischler, A. V. Poshakinskiy, S. A. Tarasenko, G. Karczewski, T. Wojtowicz, A. D. Bristow, and M. Betz, Phys. Rev. B **97**, 201413(R) (2018).

[18] S. Anghel, F. Passmann, A. Singh, C. Ruppert, A. V. Poshakinskiy, S. A. Tarasenko, J. N. Moore, G. Yusa, T. Mano,

T. Noda, X. Li, A. D. Bristow, and M. Betz, Phys. Rev. B **97**, 125410 (2018).

[19] F. Passmann, A. D. Bristow, J. N. Moore, G. Yusa, T. Mano, T. Noda, M. Betz, and S. Anghel, Phys. Rev. B **99**, 125404 (2019).

[20] S. Anghel, F. Passmann, K. J. Schiller, J. N. Moore, G. Yusa, T. Mano, T. Noda, M. Betz, and A. D. Bristow, Phys. Rev. B **101**, 155414 (2020).

[21] S. Anghel, A. V. Poshakinskiy, K. Schiller, F. Passmann, C. Ruppert, S. A. Tarasenko, G. Yusa, T. Mano, T. Noda, and M. Betz, Phys. Rev. B **103**, 035429 (2021).

[22] M. Kammermeier, P. Wenk, and J. Schliemann, Phys. Rev. Lett. **117**, 236801 (2016).

[23] D. Iizasa, D. Sato, K. Morita, J. Nitta, and M. Kohda, Phys. Rev. B **98**, 165112 (2018).

[24] D. Iizasa, M. Kohda, U. Zülicke, J. Nitta, and M. Kammermeier, Phys. Rev. B **101**, 245417 (2020).

[25] M. A. Brand, A. Malinowski, O. Z. Karimov, P. A. Marsden, R. T. Harley, A. J. Shields, D. Sanvitto, D. A. Ritchie, and M. Y. Simmons, Phys. Rev. Lett. **89**, 236601 (2002).

[26] W. J. H. Leyland, R. T. Harley, M. Henini, A. J. Shields, I. Farrer, and D. A. Ritchie, Phys. Rev. B **76**, 195305 (2007).

[27] T. Takahashi, S. Matsuzaka, Y. Ohno, and H. Ohno, Physica E **42**, 2698 (2010).

[28] J. Ishihara, G. Kitazawa, Y. Furusho, Y. Ohno, H. Ohno, and K. Miyajima, Phys. Rev. B **101**, 094438 (2020).

[29] See Supplemental Material at http://link.aps.org/supplemental/10.1103/PhysRevB.105.144412 for details on the spin distribution measured in the diffusive regime.

[30] A. V. Poshakinskiy and S. A. Tarasenko, Phys. Rev. B **92**, 045308 (2015).

[31] D. Iizasa, A. Aoki, T. Saito, J. Nitta, G. Salis, and M. Kohda, Phys. Rev. B **103**, 024427 (2021).

[32] W. J. H. Leyland, R. T. Harley, M. Henini, A. J. Shields, I. Farrer, and D. A. Ritchie, Phys. Rev. B **77**, 205321 (2008).

[33] M. P. Walser, U. Siegenthaler, V. Lechner, D. Schuh, S. D. Ganichev, W. Wegscheider, and G. Salis, Phys. Rev. B **86**, 195309 (2012).